this stage. However, if drive pillars are removed, or percentage extraction in the area is great, then stone walls will eventually take the greater proportion of the support load. Furthermore, due to the greater area of the stone wall it has a greater effect on ride and general hangingwall stability. Sand filling and power stowing, due to the greater material compaction, carry higher loads for less closure than the stone wall.

4.3 <u>Support Pillars:</u>

If pillars are solid, their load deformation characteristics should correspond to that of the solid rock specimens tested in the laboratory. If pillars are fractured, the deformation of the pillars will increase greatly, and finally, in the broken up stage, pillars may be expected to behave in a manner similar to stone walls. The present research programme has been implemented to study pillar stresses and pillar deformation under mining conditions.

5. LABORATORY TESTS

The objectives of the laboratory tests were to determine :-

(i) the elastic properties and strengths of St. Helena rock samples;

(ii) the stress distribution around a model of a St. Helena stope by photo-elastic analysis;

(iii) the stress and closure around a stope excavation for different methods of mining simulated on the Resistance Analogue.

5.1 Rock Testing:

Dynamic and static tests were made on several types of Quartzites in the geological succession above and below the Basal reef horizon. The equipment used for these tests was the Ultrasonic Tester and the Amsler Compression Machine.

5.1.1 The Ultrasonic Tester:

The Ultrasonic Tester consists of an electrical vibrator which passes ultrasonic pressure waves through a rock sample. An oscilloscope is used to measure the time taken for the waves to pass through the rock sample. The relationship between the speed of this wave (V) and the dynamic modulus of elasticity (E_d) is given below :-

$$V^2 = \frac{E_d}{\text{Density}} \frac{(1-n)}{(1+n)\quad(1-2n)}$$

By using an average value for Poissons ratio (n) of 0.14 for St. Helena Quartzites, the above equation becomes approximately :-

$$E_d = V^2 \text{ density}$$

Eighteen samples of 1 in. diameter diamond drill core were selected for testing. These samples represented a hundred feet of the geological sequence above and below the Basal reef plane. A specimen

9 ins. long /.....

9 ins. long was cut from each sample and the ends of the specimen were ground flat. The dimensions of the specimens were measured using calipers and each specimen was weighed on a laboratory balance. From the volume and weight of each specimen its density was calculated. Each specimen was then located between the terminals of the electrical vibrator, and the time for the ultrasonic wave to pass along the length of the specimen was measured on the oscilloscope. The propogational velocity of the ultrasonic wave was calculated from the specimen length and the measured time. The dynamic modulus was then calculated by substituting the value of the wave velocity and the rock density into equation 14.

The values of Young's Modulus for the eighteen specimens tested are given in Table 1. Nine of the same specimens were later sent to the C.S.I.R. for destructive testing, and the results of these tests are given for comparison in Table 1. The comparison shows that for two of the specimens the results obtained in the static tests were the same as those obtained by dynamic testing. Two results were within 4 per cent and four results were within 13 per cent. Thus, for practical purposes, the sonic tester can be considered to give sufficiently accurate results.[11]

Table 1 shows that there is a difference of up to 50 per cent between values of Young's Modulus for the specimens of the same geological classification. This difference may be due to slight variations in pebble content and matrix composition which are not taken into account in normal geological classification. Where the pebble content is less variable, as in the footwall quartzite, the percentage difference in Young's Modulus is much less (9 per cent).

5.1.2 <u>The Amsler Compression Machine:</u>

Nine samples obtained from two diamond drill holes in 2326 cross-cut were prepared for testing in the Amsler compression machine. Six of the samples were 1.66 ins. in diameter and were cut to a length of 3.2 ins. The remaining three samples were 2.12 ins. in diameter

and / ......

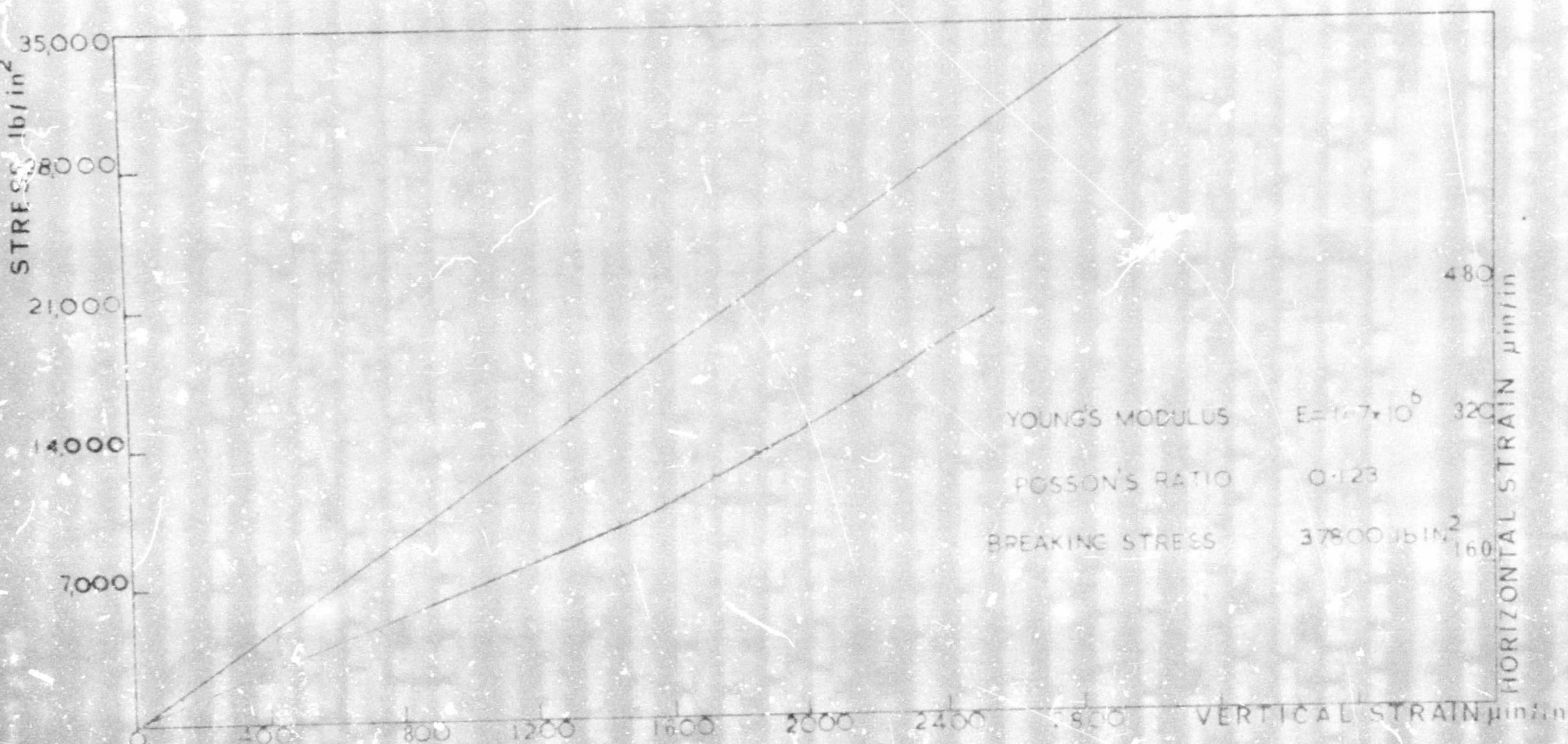

FIG 19

Uniaxial Compression Test on BASAL REEF Quartzite and were cut to a length of 4.2 ins. The ends of the nine specimens were ground flat in the oscillating grinding machine, and the length and diameter measured with calipers. Four strain gauges were then cemented diametrically opposite and mid-way along the length of each specimen. Two of these gauges indicated the horizontal strain and the remaining two the axial strain. Each pair of gauges was connected to form an arm of an electrical bridge and the gauges of another specimen were used as compensating gauges in the second arm of the bridge. The circuit was completed by connecting to a Huggenburger strain indicator. Balancing of the bridge to give null deflection enabled a direct strain reading to be obtained for any value of the applied stress. The test specimen was placed between the platens of the compression testing machine and carefully centralized. A constant loading rate was applied and strain readings were taken at fixed intervals of load until fracture occurred. The maximum load reading at fracture was taken to be the uniaxial compressive strength of the rock.

For each of the nine specimens tested a graph was plotted of stress against axial strain and the value of Young's Modulus obtained from the slope of the graph. FIG. 19 shows the stress-axial strain relationship and the axial-horizontal strain relationship for one of the specimens. Poisson's ratio was obtained from the slope of the curve of horizontal strain plotted against axial strain. The values of Young's Modulus and Poisson's ratio for the nine specimens are given in Table 2.

The results of the compression tests show that the quartzitic specimens are elastic, FIG. 19, being a typical result. It can be seen from Table 2 that the values of Young's Modulus for the six Basal reef specimens are in close agreement, and the arithmetic average was used in the equation for the calculation of underground stress. The values of Poisson's ratio for the Basal reef quartzites was more variable, but the average value was used in the same stress calculations. The underground measurements of stress were made in the same area as that from which laboratory samples were obtained.

The / ......

The value of the uniaxial compressive strength for the Basal reef quartzite varied between 28,000 lb./in.^{2} and 42,000 lb./in.^{2}

5.2 The Determination of the Principal Stress Distribution around a Model of a St. Helena Stope Excavation:

The principal stress distribution around a mine model is most conveniently determined by a photo-elastic analysis[12]. The results of this analysis are obtained in terms of the difference between the major and minor principal stresses. These stresses are then separated by the use of a resistance paper analogue.

Photo-elastic stress analysis is carried out in a polariscope which uses plane or circular polarized light to form an interference pattern around a stressed model. Models are made from photo-elastic material by milling or cutting. The use of circular polarized light produces an interference pattern which corresponds to the contours of equal principal stress difference only, isochromatic lines. If plane polarized light is used, an interference pattern is produced, showing isochromatic and isoclinic lines. The latter are used to find the directions of the principal stresses. Most polariscopes have a lens and camera arrangement for photographing interference patterns.

The material used for the St. Helena model was Columbia resin (C.R.39). A model of a cross-section of a typical St. Helena stope and drive, including the internal stope pillars, was milled from this material. This model was placed in the polariscope and stressed to a load of 620 lbs. By using light and dark fields photographic negatives were obtained of the half order and whole order isochromatic fringes. These two negatives were used in conjunction with the resistance paper analogue to separate the principal stresses. The calculations of nominal fringe order and of the stress difference at any point in the model are given in APPENDIX IA.

The analogue paper technique depends on the fact that the voltage distribution in a uniformly conducting sheet, and the sum of the principal stresses in a plane stress field, satisfy La Place's equation. The voltage distribution relationship is given by :-

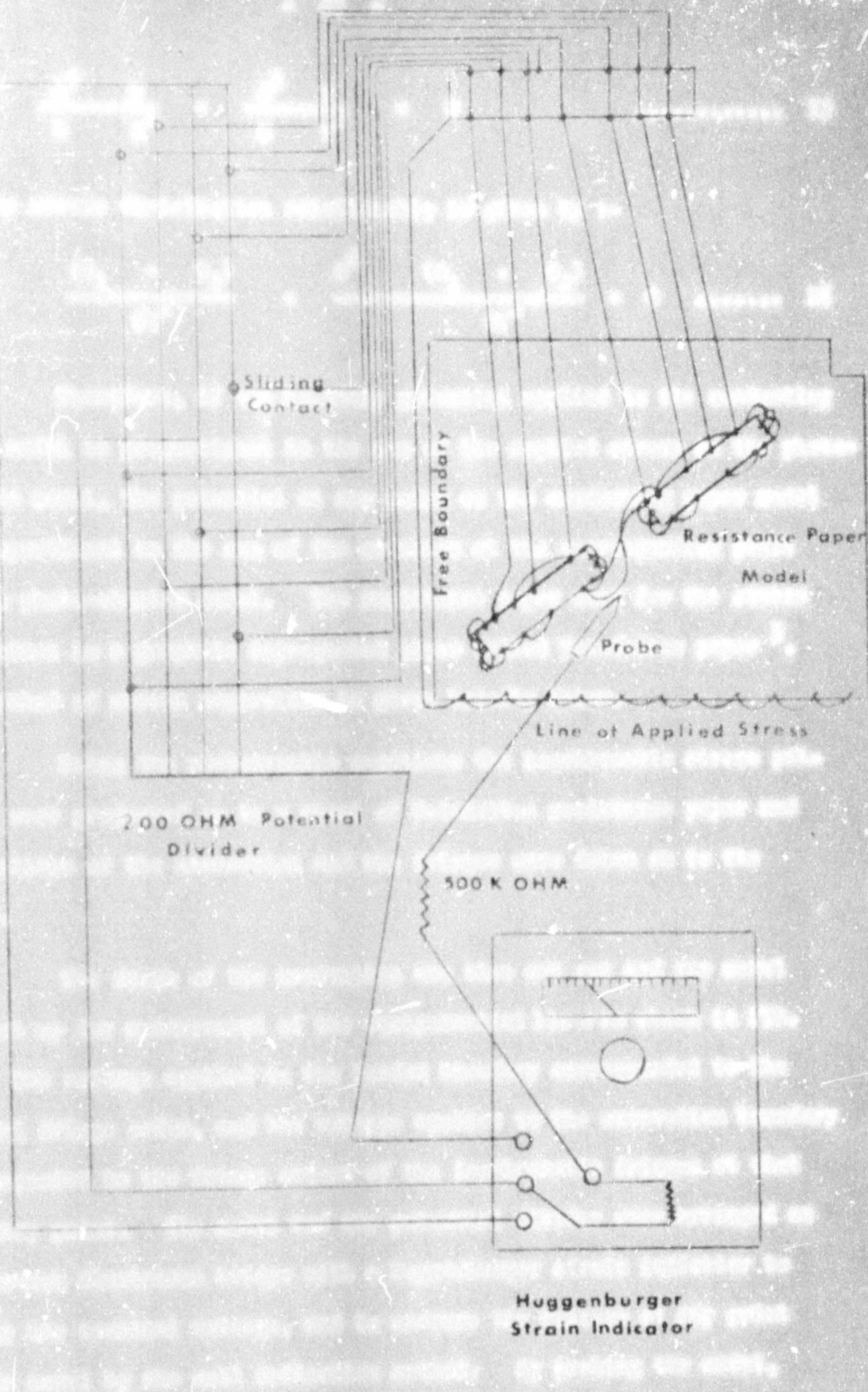

FIG 20

Layout for Resistance Paper Analogue Test

$$\frac{\partial^2 V}{\partial X^2} + \frac{\partial^2 V}{\partial Y^2} = 0 \quad \ldots\ldots\ldots\ldots \quad 15$$

and the stress distribution relationship is given by :-

$$\frac{\partial^2 (\sigma_1 + \sigma_2)}{\partial X^2} + \frac{\partial^2 (\sigma_1 + \sigma_2)}{\partial Y^2} = 0 \quad \ldots\ldots\ldots \quad 16$$

Therefore, if the boundary potential applied to the conducting paper model is proportional to the sum of the applied stress on the photo-elastic model, the potential at any point on the conducting paper model is proportional to the sum of the stresses at the corresponding point in the photo-elastic model. The resistance paper used for the stress separation is a graphite impregnated paper called Teledeltos paper [3]. The method of stress separation is given briefly below.

Using the photographic negatives the isochromatic stress patterns were projected on to a sheet of Teledeltos resistance paper and the outline of the excavation and the fringes were drawn on to the paper.

The shape of the excavation was then cut out and the model was set up for measurement of the equipotential lines as shown in FIG. 20. The voltage applied to the loaded boundary corresponded to the nominal fringe order, and the voltage applied to the excavation boundary corresponded to the fringe orders of the isochromatic fringes at that boundary point. The model and the potential divider were arranged as a four-arm Wheatstone bridge with a Huggenburger strain indicator to supply the terminal voltage, and to measure the voltage at any point on the model by the null deflection method. By probing the model, equipotential lines were drawn. As the equipotential lines are proportional to the principal stress sum, and the isochromatic fringes to the principal stress difference, the major and minor principal stresses can be separated at the point of intersection. Finally, the contours of major and minor principal stresses are obtained by joining points of equal stress magnitude. Shear stress contours are

identical / ......

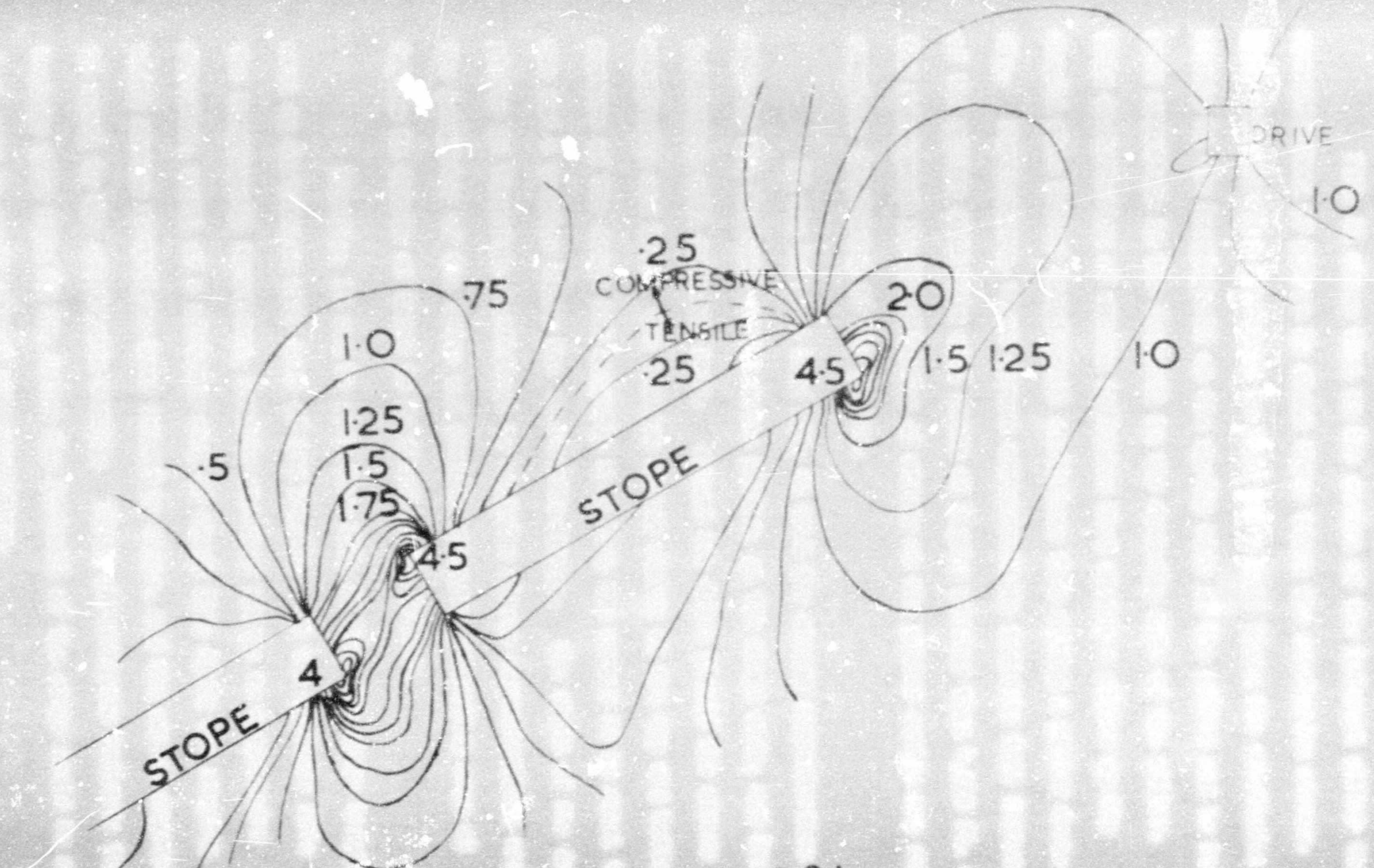

FIG 21

CONTOURS OF MAJOR PRINCIPAL STRESS
EXPRESSED AS RATIOS OF σ/p

identical to the isochromatic pattern, since the latter is proportional to the principal stress difference. The contours of the major principal stresses and the shear stress round a St. Helena stope excavation are shown in FIGS. 21 and 22.

FIG. 21 shows that in the centre of the internal pillar the concentration of stress is about three times the overburden stress. This concentration increases to four and a half times the overburden stress in the hangingwall on the up-dip side of the pillar and to the same magnitude in the footwall in the down-dip side of the pillar. This distribution of stress indicates that mining a pillar up-dip should give better hangingwall conditions than mining a pillar down-dip. Furthermore, these stress concentrations indicate that failure of the pillar sidewalls will occur at depths greater than 4,000 ft. and the subsequent re-distribution of stress at the pillar centre may cause complete fracturing of the pillar.

It can be seen from FIG. 21 that the stress concentration is high in the footwall of the drive pillar, on the stope side, and fracture initiation will commence here. Around the drive itself the stress magnitudes are low. The maximum stress occurs at the top and bottom corners of the drive and slightly away from the corner it is equal to one and a quarter times the overburden stress. The width of the drive pillar is therefore sufficient to minimise stress concentrations around the perimeter of the drive and provide adequate protection even at depths in excess of those to be mined on St. Helena.

Finally, it can be seen from FIG. 21 that the stope hangingwall is in tension over most of its length. As the distance into the hangingwall increases, tensile stresses change to compressive stresses, until at a distance away of about five times the stoping width stress variations have ceased to occur, and the stress magnitude is equal to the overburden stress. These observations indicate that a haulage more than 60 ft. below the footwall of the stope would be subject only to small stress concentrations.

5.3 Experiments / ......

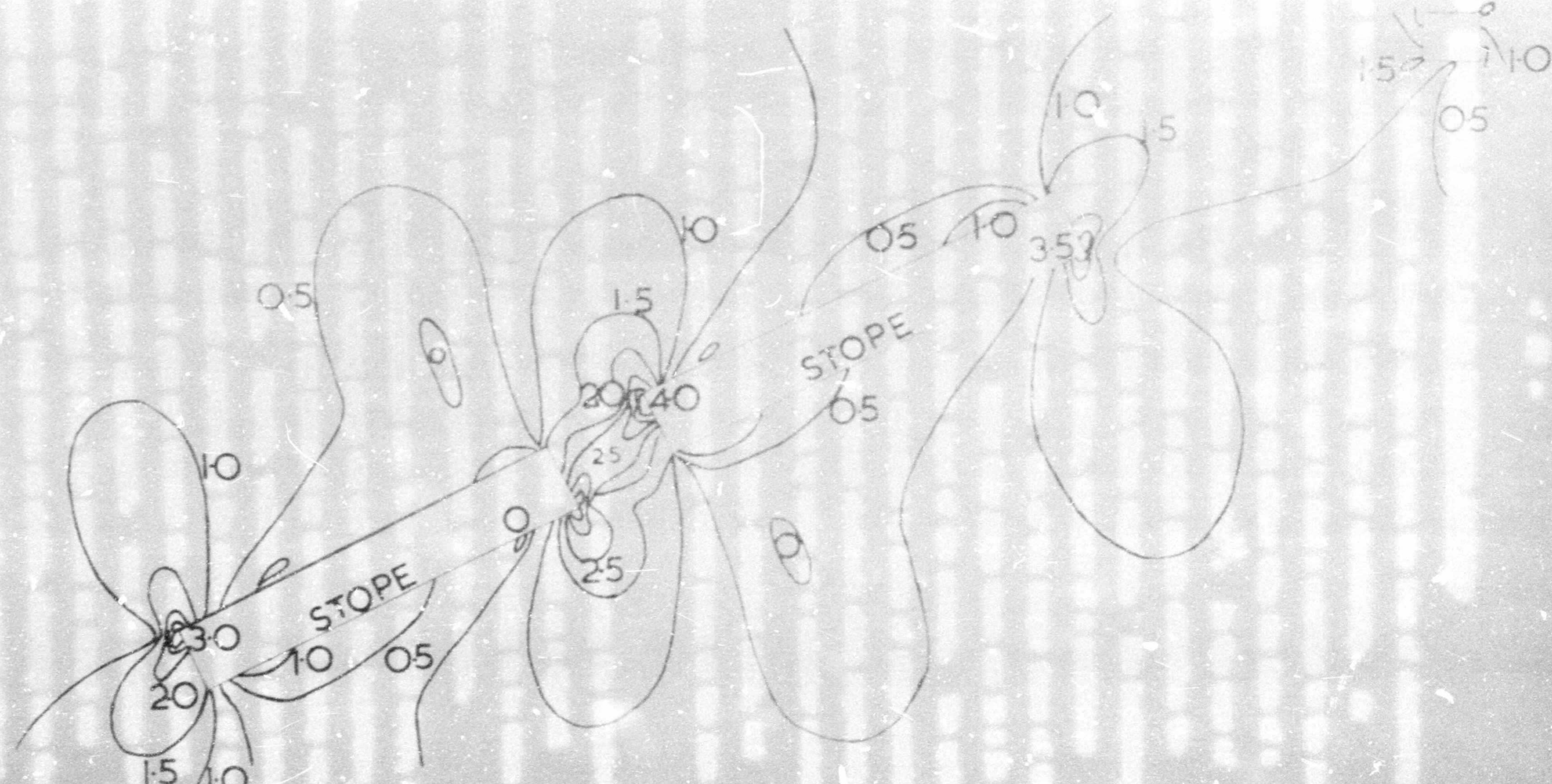

FIG 2.2

CONTOURS OF MAXIMUM SHEAR STRESSES

5.3 Experiments conducted on the Resistance Analogue:

A mathematical analogy exists between the laws of elasticity, and the equations governing the steady flow of electricity. An electrical analogue can therefore be used to find a solution to the La Place equation No. 16. This analogue can either take the form of a continuous fluid medium, or a resistance network[13]. In the case of the resistance network, the potential at nodal points satisfies the finite difference equivalent of the La Place equation. The Resistance Analogue, as used by the Chamber of Mines, consists of a resistance network occupying a rectangular prism. One of the larger faces of this prism represents the reef plane. Below this plane there are 50 X 30 resistance cubes which form the first layer of the network. The nodes of these cubes can be short or open circuited by means of plugs passing through holes drilled into the brass ground electrode which represents the reef plane. Nodes can be monitored by means of a selector switch.

Intact reef is represented by short circuited nodes, and hence the shape of the excavation appears as vacant holes on the face of the Analogue.

Stress on the reef plane is found by monitoring the required node and reading off the closed circuit nodal current on a digital voltmeter. Removal of a plug allows a potential reading to be taken on the digital voltmeter which is proportional to the closure.

As underground measurements were to be made in 2323 Stope, a plan of this stope at the ledging stage was set out on the Resistance Analogue. Closure and stress was measured as underground mining was simulated by extracting plugs. Firstly, vertical lines of pins between the drive pillars were removed representing the strike advance of the stope face. As each line of pins was removed the stress at several points along the new stope face was measured. When the distance between the stope faces was about 40 ft., the remnant so formed was mined out by advancing 30 ft. long faces on strike, starting from the down-dip side of the remnant. Thus the toe of the remnant advances

up-dip / ......

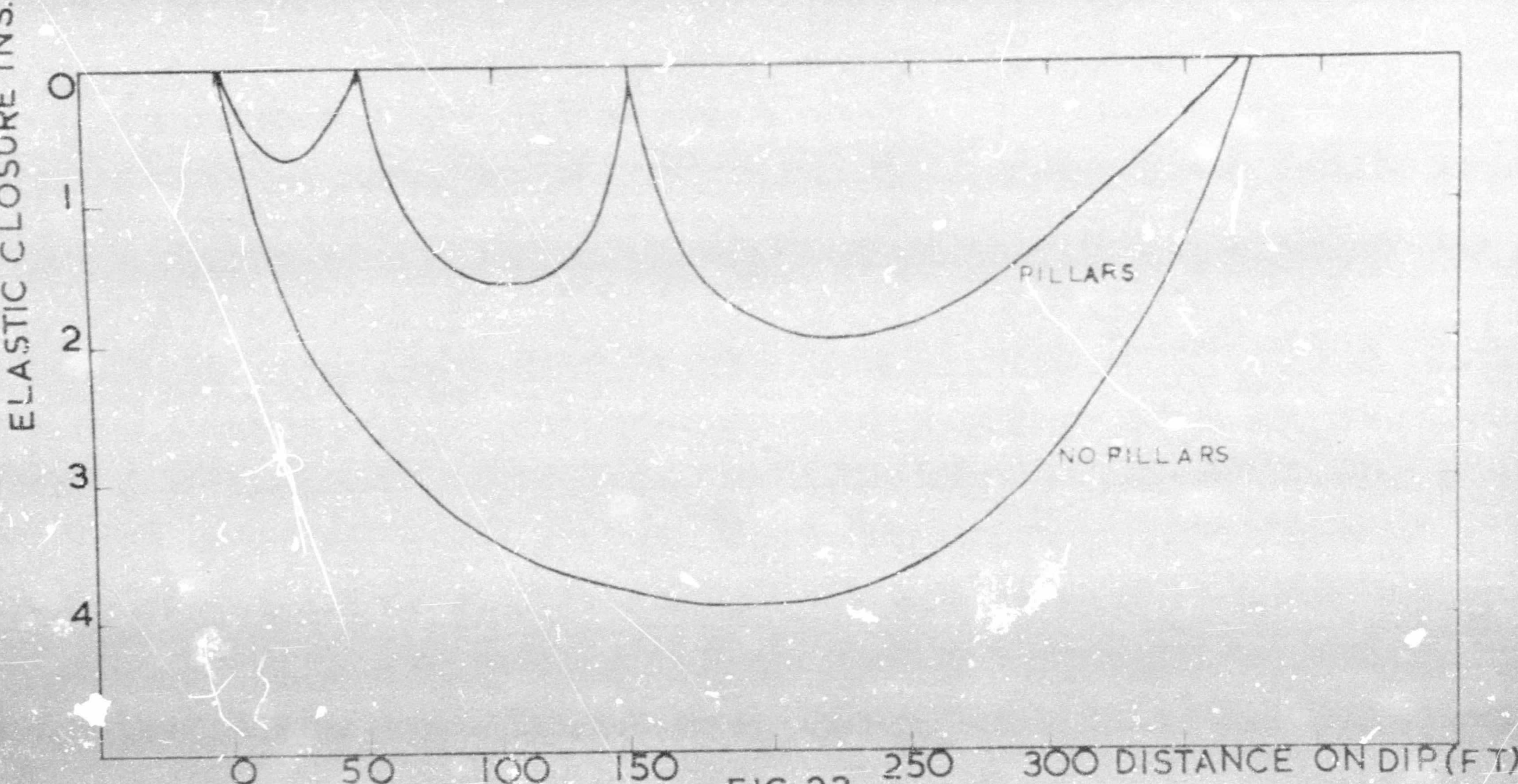

FIG 23

ELASTIC CLOSURE WITH AND WITHOUT PILLARS

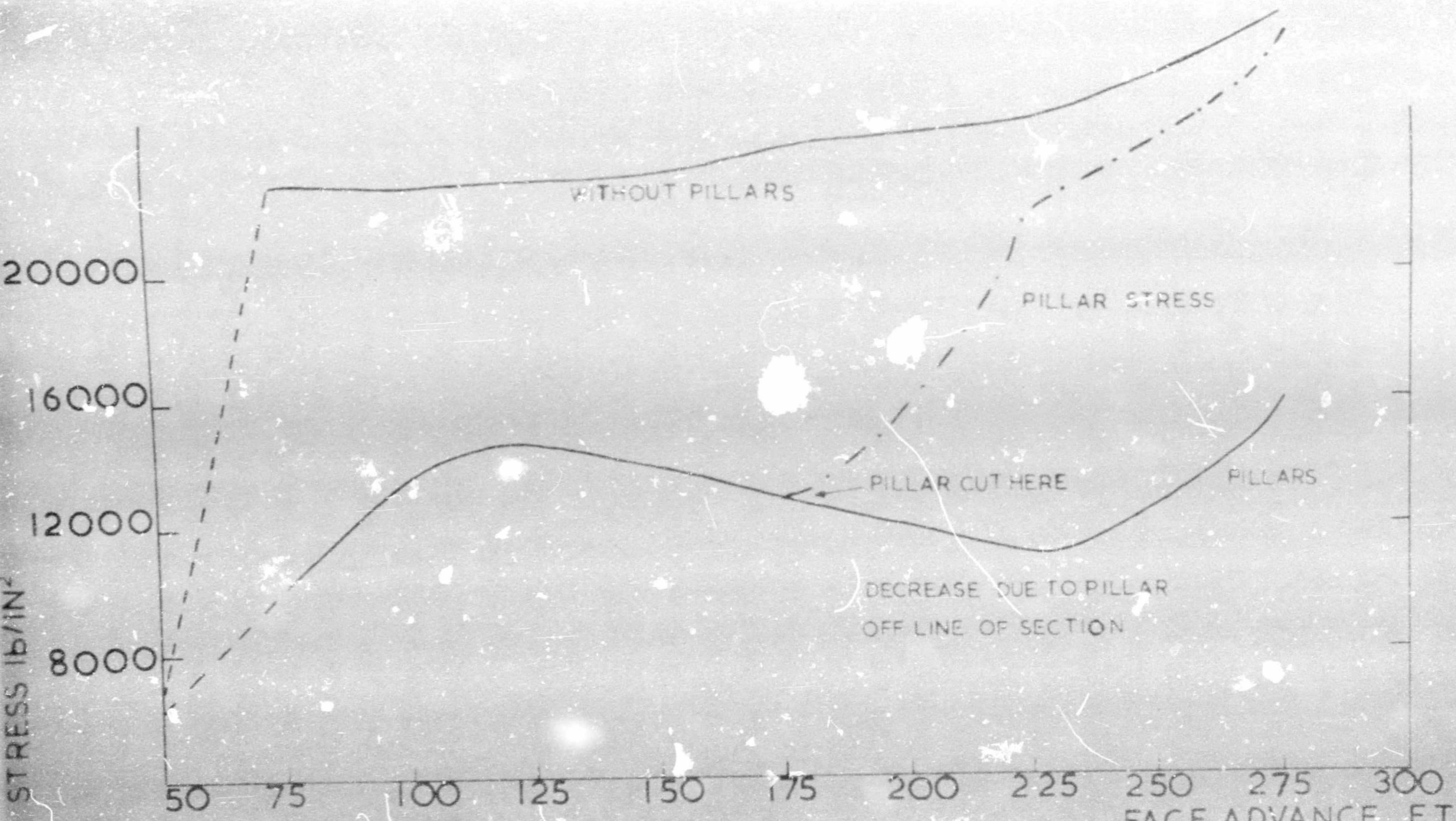

FIG 24

COMPARISON OF STRESS ON THE STOPE FACE

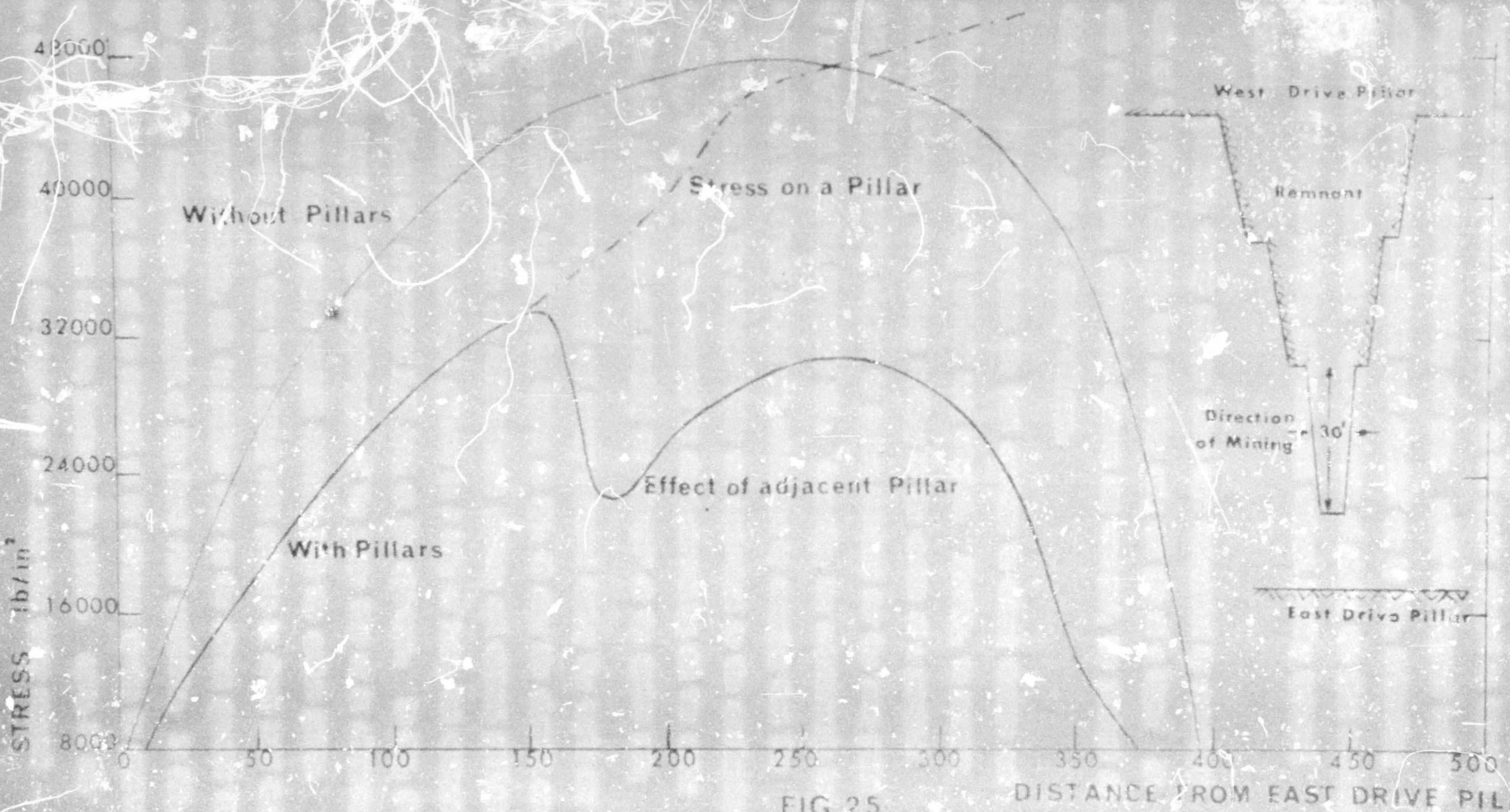

FIG 25

Stress on the Toe of the Remnant as it is Mined Up Dip up-dip in steps of 30 ft. The stress on the toe of this remnant was measured as extraction proceeded. On the scale adopted an internal stope pillar was represented by one pin. After the remnant had been extracted the internal pillars were removed one by one, retreating towards the original raise. This sequence of mining was then repeated commencing from the ledging position, but without leaving internal pillars.

Finally, energy release rates were calculated by repeating both of the above methods, but removing only one pin at a time. As each pin was removed, stress and closure was measured, the product of which gave the rate of energy release.

In order to relate the test readings to actual closure and stresses, the following methods were adopted. Firstly, to measure simulated closure, the voltage reading at the centre of a parallel slit was equated to the closure in inches obtained for the same point by analytical solution (APPENDIX II). Secondly, the relationship between current and actual stress was calculated by assuming that the residual current on the Analogue Tutor was equivalent to the overburden stress. This current was measured by short-circuiting all the nodes on the face of the Tutor and reading the "stress" at the centre pin.

The closure, stress and energy measured during the tests are plotted on FIGS. 23 to 30. The curves in FIG. 23 show the closure occurring on a line of true dip with internal pillars and without pillars. Maximum closure between internal pillars is 2 ins. or less, but without internal pillars the closure is 3.88 ins. at the mid-span. In FIG. 24 the stress magnitudes on the mid-point of the stope face as it advances on strike, are shown plotted against distance from the centre gully. The stress on the stope face when mining with pillars is about half that of mining without pillars, but in neither case is the stress greater than the uniaxial compressive strength of the Basal reef quartzite. In FIG. 25 the stress on the toe of the remnant as it advances up-dip is plotted against distance in feet from the bottom drive pillar. Again it can be seen that stresses on the stope face are less when using support

pillars / ......